Methods: One hundred and thirty-nine females (55—94 years) and sixty males (60—93 years) who had sustained atraumatic hip fractures underwent QCT scans within 48 hours of the fracture, and we used BIT software which directed automatic the lowest area the mid-femoral neck cross-section perpendicular to the femoral neck axis to measure cortical thickness (C.Th) in anatomic quadrants of the femoral neck.
Results: For elderly females, the estimated C.Th in superoanterior (SA) quadrants, inferoanterior (IA) quadrants, inferoposterior (IP) quadrants and superoposterior (SP) quadrants were (0.90±0.61) mm, (2.20±0.83) mm, (3.70±0.96) mm and (0.85±0.54) mm respectively, for elder males the corresponding parameters being (1.33±0.71) mm, (2.22±0.90) mm, (3.72±0.79) mm and (1.20±0.79) mm. Although the elderly females had significantly thinner mean C.Th in SP and SA quadrants than the parameters of the males ($p<0.05$), the sexes did not differ in cortical thickness in IA and IP quadrants. Comparing age-related decrease changes of C.Th in anatomic quadrants for females, there was no age-related changes for males.
Conclusion: When comparing males and females in our study, there is no difference in C.Th in infero quadrants, but women have thinner C.Th in supero quadrants. Thinner cortical thickness in the superior region of the femoral neck may be a stronger predictor for hip fracture, implying the mechanism causes a higher fracture incidence in women.

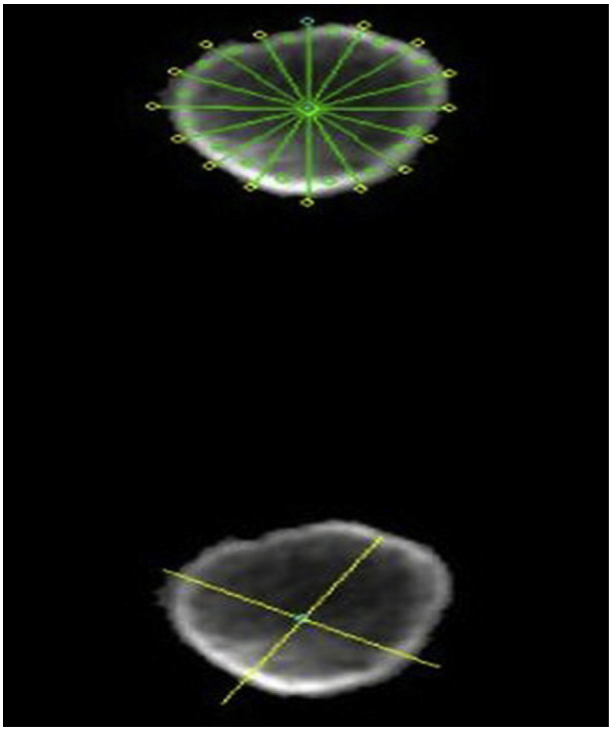

IBDW2014-00153-F0074
DECONVOLUTION-BASED FORWARD MODEL APPROACH FOR IMPROVED ACCURACY OF VERTEBRAL CORTICAL THICKNESS BASED ON CT DATA OF DIFFERENT QUALITY (QCT, HR-QCT AND HR-pQCT)

T. Damm, J. Pena, J. Bastgen, G. Campbell, R. Barkmann, C.-C. Glueer
Department of Radiology and Neuroradiology, University Hospital Schleswig-Holstein, Kiel, Germany

Objective: Bone stability is influenced both by cortical and cancellous bone mineral density (BMD), structure and mineralization status. Computed tomography (CT) permits assessment of these characteristics and can be used for individual fracture risk assessment as well as for longitudinal studies monitoring of treatment effect. New therapies may not only improve the cancellous bone, but also strengthen the rather compact cortex, where this is achievable by endosteal or periosteal apposition, increasing mineralization, or reduction in resorption space. To assess bone parameters on clinical CT data, one has to deal with limited spatial resolution and significant partial volume effects, which heavily blur this very thin structure (typically 150-350μm, Ritzel 1997).
Methods: We analyzed CT data of 9 excised embedded vertebrae scanned using 3 different CT protocols (fig. 1): (I) High Resolution peripheral Quantitative CT (HR-pQCT) (Scanco Medical Xtreme CT, voxel size (0,082*0,082*0,082)mm^3, 60kV, 190mAs) used as gold standard, (II) High Resolution Quantitative CT (HR-QCT) (Siemens Sensation64, voxel size (0,156*0,156*0,300)mm^3, 120kV, 360mAs) and (III) Quantitative CT (QCT) (Siemens Sensation 64, voxel size (0,234*0,234*1,000)mm^3, 120kVp, 100mAs).
We developed a method for measuring radial BMD profiles along the cortex (i.e. density distribution orthogonal to the cortical surface) based on cortical segmentation as part of our quantitative CT analysis software StructuralInsight (ITK-based). Using a priori knowledge of vertebral skeletal structure by fitting a radial BMD profile to the measured data directly returns a deconvolved cortical thickness (dcCt.Th) and the CT system's point spread function (PSF) as a measure of spatial resolution. For comparison we also calculated a direct maximum-sphere based cortical thickness (Ct.Th) and, as a simple correction for partial volume effects, weighted cortical thickness (wCT.Th = cortical BMD x CT.Th).
Results: Cortical thickness by HR-pQCT was (370±70)μm. Compared to these results the table shows the mean offsets and the root mean square errors (RMSE) of QCT and HR-QCT based estimates. Here dcCt.Th shows very low random residual errors even in QCT data analysis.
Conclusion: Our results document that uncorrected cortical thickness of 370 μm is overestimated by factors of 4.8 and 4.2 by QCT and HR-QCT at measured levels of (1.78±0.58)mm and (1.54±0.29)mm respectively. This factor can be reduced to 1.4 or 1.2 by dcCt.Th to levels of (522±93)μm and (434±71)μm, respectively, and the residual error is reduced to 36μm and 17μm respectively, for the two techniques. For accurate modeling of mechanical strength such corrections are of specific importance.

IBDW2014-00154-F0075
3D ANGIOARCHITECTURE OF SPINAL CORD IN A RAT MODEL DETECTED BY SYNCHROTRON RADIATION MICRO-COMPUTED TOMOGRAPHY

Yong Cao [a], Jianzhong Hu [a], Tianding Wu [a], Dongzhe Li [a], Hongbin Lu [b]
[a]*Department of Spine Surgery, Xiangya Hospital, Central South University, Changsha 410008, China*
[b]*Department of Spine Surgery, Xiangya Hospital, Central South University, Changsha 410008, China*

Objective: A high-resolution three-dimensional (3D) visualization of spinal angioarchitecture is essential to reveal its pathomorphological alterations causing the dysfunction of the local microcirculation in the neural parenchyma. However, acquiring such high-resolution vascular imaging remains an experimental challenge. Herein, we used the high-resolution X-ray attenuation imaging based on the synchrotron radiation coupled with angiography to reconstruct the vessel skeleton of spinal cord digitally.
Methods: This method was applied to a rat model of traumatic spinal cord injury using a modified Allen's weight drop apparatus. Following vascular perfusion with contrast agent, the T10 thoracic cord segment (about 6mm) was harvested and scanned by synchrotron radiation micro-computed tomography.
Results: With a minimum resolution as 3.7μm, the 3D vascular architecture of rat spinal cord was reconstructed optimize and quantified (Fig 1). Compared with conventional histological sections, the reconstructed images were consistent with that obtained from histomorphology sections. Meanwhile, the vascular pathological change after spinal cord injury could be reflected by some characteristic parameters (Fig 2).
Conclusion: In summary, the high-resolution X-ray attenuation imaging based on the synchrotron radiation coupled with angiography is a potential and powerful tool to investigate the 3D neurovascular morphology of the rat spinal cord. It could help to evaluate the angiogenesis on microvasculature repair or regeneration research.

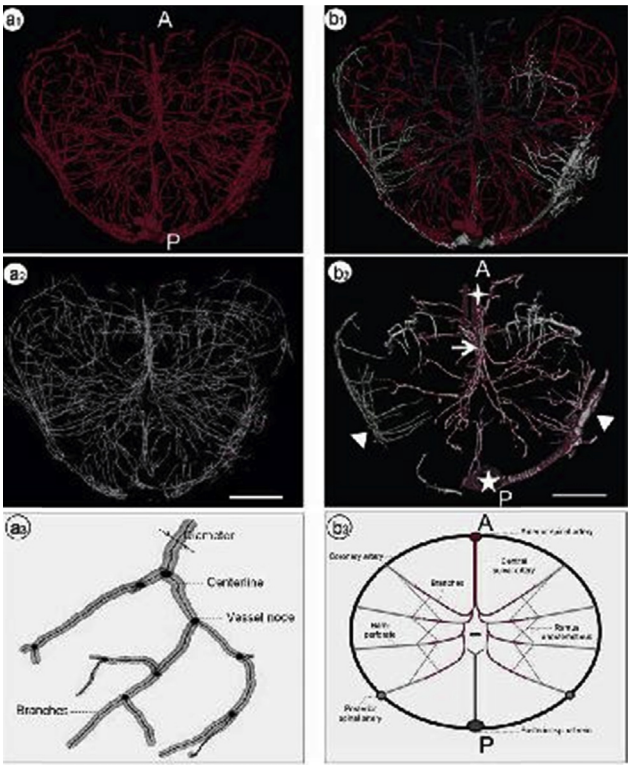

Fig. 1 (a) Synchrotron radiation image optimization, (a1) The whole 3D volumetric rendering of the intact vasculature of the normal spinal cord segment. (a2) The centraxonial vessel skeleton was abstracted from the 3D spatial angioarchitecture. (a3) The illustration to characterize the vascular branch feature with a simulative analytical model. Fig. 2 (b) Vascular arrangement of blood supply in spinal cord. (b1-2) The pseudocolors were painted to display the different administrative region from the top view. (cross=ASA; triangle=PSA; arrow=CSA; star=PSV; ba=500 μ m) (b3). A manual drawing to simulate the blood supply pattern of rat normal spinal cord. (A=anterior; P=posterior).

IBDW2014-00155-F0076
A NOVEL STUDY BY CONFOCAL RAMAN MICRO-SPECTROSCOPY IN THE RABBIT BONE-TENDON JUNCTION OF THE PATELLA-PATELLAR TENDON

Zhanwen Wang, Ziteng Zeng, Cheng Zheng, Jingyong Zhou, Jianzhong Hu, Hongbin Lu
Department of Sports Medicine and Research Center of Sports Medicine, Xiangya Hospital, Central South University, Changsha, PR China

Objective: With confocal Raman micro-spectroscopy, we tried to distinguish different structures of rabbit patellar-patellar tendon junction (PPT) and explore the new method for further study to evaluate bone tendon junction healing.
Methods: The PPT samples were harvested carefully from four healthy bone matured male New Zealand rabbits cadavers and were sectioned crossing the median sagittal plane. All samples underwent no chemical treatment for Raman analysis. After all the Raman spectra were acquired, baseline correction for each individual spectrum was performed. The relative peak intensity of 960Δcm-1 standing for mineral and 2940Δcm-1 for collagen as well as mineral-to-collagen ratio (960Δcm−1/2940Δcm- 1) was used as indicators to identify which structure the scanning spot belongs to. Meanwhile, through X-axis coordinate of each individual position, the thickness of the junction in rabbit PPT can be calculated. After Raman spectroscopy scanning, the PPT samples were observed optically in histological sections (HE staining).
Results: According to Raman analysis, three different yet continuous structures of PPT could be well identified: bone, fibrocartilage, and tendon (Fig 1A). The thickness of fibrocartilage was about 1800μm. This result was highly consistent with histological study. The collagen content (the peak intensity strength of 2940Δcm-1) in bone was higher than tendon (Fig 1A). We also found that the mineral-to-collagen ratio gradually increased across the junction from the tendon to bone. The 960Δcm-1 band across the junction became narrow in the same mineral zone. Interestingly, we found that combined with histological observation, some scanning spots around the tidemark showed higher mineral-to-collagen ratio than bone (Fig 1B). This might be the result of the process of continuous and dynamic mineralization existing around the boundary (i.e., tidemark) region.
Conclusion: Confocal Raman micro-spectroscopy could be used to distinguish and measure the thickness of the classic structures of the PPT samples. Furthermore, it could detect the distribution and the degree of mineralization as well as the content of the organic tissue (almost collagen I) across the tendon−bone junction.
Acknowledgement
This work was supported by The National Natural Science Foundation of China (No. 81171699).
B: Mineral/Collagen Ratio of each spectrum in A.

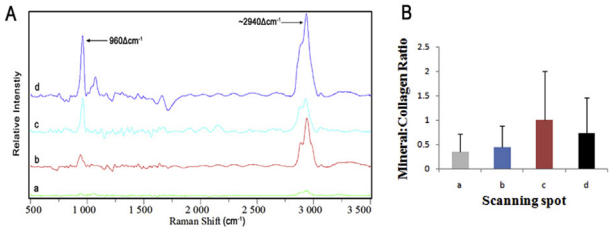

Fig 1. A: The classical spectra of sample #2. Spectrum ***a*** represented for tendon, ***b&c*** for fibrocartilage and ***d*** for bone. The position of spectrum ***c*** was around the timemark. Mineralization increased from tendon to bone. The collagen content in bone was higher than tendon.

IBDW2014-00156-F0077
CHARACTERIZATION OF ZINC AND CALCIUM SPATIAL DISTRIBUTION AT THE FIBROCARTILAGE OF RABBIT PATELLA-PATELLAR TENDON COMPLEX: A SYNCHROTRON RADIATION MICRO X-RAY FLUORESCENCE STUDY

Can Chen [a], Zhanwen Wang [a], Cheng Zheng [a], Tianding Wu [b], Yong Cao [b], Hu Jianzhong [b], Yi Zheng [a,b], Hongbin Lu [a]
[a]*Department of Sports Medicine, Research Center of Sports Medicine, Xiangya Hospital, Central South University, Changsha, Hunan, PR China*
[b]*Department of Spine Surgery, Xiangya Hospital, Central South University, Changsha, Hunan, PR China*

Objective: Zinc (Zn) and calcium (Ca) play important roles in the normal growth, remodeling and mineralization of fibrocartilage zone of patella-patellar tendon complex (PPTC). Synchrotron radiation micro X-ray fluorescence (SR-μXRF) allows in situ mapping of Zn and Ca at nanometer level with high sensitivity. Therefore, the main purpose of this study was to characterize the distribution of Zn and Ca at the fibrocartilage zone of PPTC.
Methods: (1) Sample Preparation: Four PPTC of rabbits were embedded with polymethylmethacrylate and cut sagittally with a thickness of 100μm. (2) Backscattered electron imaging (BEI): An electron-probe microanalyzer was utilized to acquire BEI images. The region of interest and tidemark (TM) of PPTF were determined based on the BEI images (Fig.1.A). (3) SR-μXRF: the distribution of Zn and Ca at the fibrocartilage zone of PPTC were examined at BL15U1 (Shanghai Synchrotron Radiation Facility, China) and analyzed with Igor pro program (Version 6.1, WaveMetrics, Inc, USA).
Results: (1) The distribution of Zn and Ca at the fibrocartilage zone of PPTC was successfully visualized by using SR-μXRF. The spatial resolution of elemental mapping was as small as 3 μm (Fig. 1.B). (2) The distribution of Zn and Ca at the fibrocartilage zone of PPTC was inhomogeneous. The content of Zn in the TM zone was 2.8 times higher than that of patellar tendon (Fig.1.D) (Fig.2.D). The position of highest Ca content (21.9 times of that of patellar tendon) was located in the calcified fibrocartilage zone and is about 100μm far from where the highest Zn content is. Most importantly, Ca was distributed in a gradually decreasing manner from bone to tendon